Video-based Metrology of Water Droplet Spreading on Nanostructured Surfaces

S. Cheng[1], X. Luo[2], S.M. Bhandarkar[1,2], J. Fan[3] and Y. Zhao[3]
[1]Artificial Intelligence Center, [2]Dept. of Computer Science, [3]Dept. of Physics and Astronomy
The University of Georgia, Athens, Georgia 30602, USA
canada@uga.edu, xingzhi@cs.uga.edu, suchi@cs.uga.edu
phfan@physast.uga.edu, zhaoy@physast.uga.edu

Abstract

Dynamic wettability of a nanostructured surface is an important property for many liquid-related applications of nanostructures. The dynamic wettability analysis is performed by measuring the evolution of the precursor (outer rim) contour of a water droplet as it spreads on a nanostructured surface. A video-based metrological system based on the snake active contour model which is capable of precisely tracking the precursor contour of a spreading water droplet in a high frame-rate video is developed. The radius of the precursor contour is empirically observed to obey a power law with respect to time. Experiments show reasonable agreement between the results of the metrological system and those obtained via manual measurement.

1. Introduction

Wettability measurement of a solid surface is a topic of great importance in a variety of problem areas ranging from ink-jet printing, painting, corrosion, biofoiling, DNA immobilization, cell growth, and tissue engineering. The wettability of a surface is affected by both the surface chemistry and topography. It has been demonstrated that a micro/nano patterned surface can greatly alter the surface wettability such that a hydrophobic surface becomes more hydrophobic and a hydrophilic surface becomes more hydrophilic [10]. Moreover, superhydrophobic surfaces (contact angle $> 150°$) have been achieved by treating nanostructured surfaces with chemicals which have low surface energies [9]. The surface contact angle was observed to provide a quantitative measure of the *static* wettability properties of the surface.

In addition to the measurement of static surface wettability properties, namely the contact angle described above, the dynamic spreading of a water droplet on flat, rough or porous surfaces has also been studied quite extensively [1, 2, 3, 4, 7, 14, 15]. Most investigations have addressed the evolution of a liquid droplet over time, and it is believed that the radius of the droplet R versus time obeys a simple power law, $R \propto t^{\alpha}$, where α is the characteristic of a spreading regime due to a specific underlying physical mechanism. For example, for a flat surface, α usually takes a value between $^1/_{10}$ and $^1/_8$, depending on whether the dominant driving force is the capillary force or the gravitational force [1, 2, 3, 4, 6, 7, 14, 15]. For a rough or porous surface, the spreading process becomes more complex and therefore, parameters such as the roughness or porosity of the substrate and the viscosity of the liquid have to be considered.

So far, there is still no systematic study of the dynamic spreading of liquids on nanostructured surfaces [5]. Depending on the detailed surface structure, one could treat a nanostructured surface either as a rough surface or as a porous surface. It would be interesting to know if the spreading of a liquid droplet on such nanostructured surfaces follows a similar dynamic scaling law as is observed for rough or porous surfaces. The study has the potential to provide useful surface wettability information for applications that involve the interaction of liquid droplets with nanostructures. For most dynamic spreading studies, CCD cameras are used to track the evolution of the water droplet on the surface. This kind of image/video-based metrology offers a non-contact and nondestructive means to study the wettability properties of nanosurfaces. One of the primary advantages of image/video-based metrological techniques is that they entail minimal or no perturbation of the physical quantity being measured. However, one of the major challenges posed by image/video-based metrological techniques in the study of the dynamics of the spreading of a water droplet on a nanostructured surface is the prohibitively large data processing requirement. In our study, the spreading of water droplets on Silicon nanorod arrays is recorded using a CCD camera with a very high shutter speed, capable of acquiring 210 frames per second (fps) at VGA frame resolution (800×600 pixels). For a video recording of $\sim$10 seconds, which is the typical time frame for a water

IEEE Workshop on Applications of Computer Vision (WACV'07)
0-7695-2794-9/07 $20.00 © 2007 IEEE

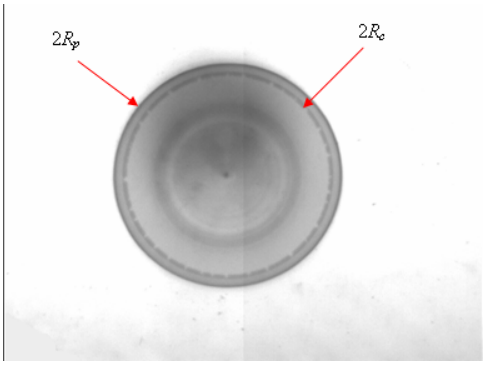

Figure 1. A single frame of the video showing a water droplet spreading on a Silicon nanorod surface. R_c and R_p are the radii of the contact line and precursor, respectively.

droplet to spread completely on a wettable surface, one obtains over 2000 video frames of data. For obtaining further information such as the instantaneous droplet spreading speed $v = \Delta R/\Delta t$, the smaller the time interval Δt, the more accurate the speed computation. Accurate measurement of the instantaneous droplet spreading speed as a function of time would therefore entail the processing and analysis of a large number of video frames. Manual processing and analysis of such large amounts of video data is onerous, error-prone and simply prohibitive. Thus, computer vision techniques for the automated processing and analysis of the video data are called for.

In this paper we describe the design and implementation of a video-based metrological system which can automatically extract and track the shape and size (dimensions) of the spreading droplets in the video frames. Section 2 outlines the employed tracking method. The experimental setup is described in Section 3, and Section 4 presents an analysis of the results.

2. Tracking of Droplet Contours in Video Frames

Figure 1 shows a typical video frame depicting the spreading of a water droplet on a nanosurface comprising of Silicon nanorods. The inner contour of the droplet, termed the *contact line*, denotes the position of the water droplet above the Silicon nanorods. The outer contour termed the *precursor*, denotes the frontal envelope of the water droplet as it spreads inside the nanorod channel. Although the outer contour of the water droplet in Figure 1 is almost circular, it could potentially deform to any shape depending the hydrophobic/hydrophilic properties and the isotropic/anisotropic nature of the nanosurface. Consequently, we model the outer contour of the water droplet using a snake which is an active contour model capable of modeling a closed contour of irregular geometry.

A snake is an energy-minimizing spline proposed by [8] for the purpose of modeling contours of irregular geometry. A snake is represented by a set of points or snake elements (snaxels) where the local and global position of each snaxel is determined by an energy function. The energy function contains terms that represent both, the external constraint forces and the internal image forces. The goal is to use the snake to find the desired image curve or contour by minimizing the energy function.

2.1. Snake Energy Function

The snake energy function is used to localize each snaxel within the image. Typically, the energy function is divided into two primary components: external energy and internal energy. The external energy is governed by image forces that attract the snaxels towards high-level image features such as points, lines, and edges [8]. Since our research focuses primarily on image contours, the natural choice for the external energy term is based on an edge function computed using an edge detector. The internal energy, on the other hand, determines the overall contour shape and generally consists of first-order and second-order terms where the first-order term influences the continuity of the snake and the second-order term influences the curvature of the snake.

The total energy $E(S)$ of the snake S is defined as the sum of the total energy value $E(p_i)$ (internal energy + external energy) of each snaxel p_i as in Equation (1).

$$\begin{aligned} E(S) &= \sum_{i=1}^{N} E(p_i) = \sum_{i=1}^{N} [E_{Int}(p_i) + E_{Ext}(p_i)] \quad (1) \\ &= \sum_{i=1}^{N} [\alpha E_{Cont}(p_i) + \beta E_{Curv}(p_i) + \gamma E_{Ext}(p_i)] \end{aligned}$$

where the weights α, β, and γ represent the contribution of the corresponding energy term to the overall energy of the snake. In summary, the energy function is used to locate (external energy) and shape (internal energy) the snake within an image.

2.2. Snake Finding Algorithm

The snake finding algorithm (Algorithm 1) is an iterative process and can be described as a greedy search in the space of potential splines [8]. The initial snake is generated in the proximity of the feature of interest either through user interaction or using an image processing algorithm such as an edge map which can localize the desired feature. The snake

finding algorithm progresses by updating each snaxel with a member within the snaxel's $M \times M$ neighborhood that minimizes the energy function. The algorithm terminates when the snake has settled sufficiently into a local minimum or it has reached the maximum number of iterations.

Algorithm 1 Snake Algorithm

1. Initialize a snake $S^0 = \{p_1^0, \ldots, p_N^0\}$ in the proximity of the desired image feature.
2. At iteration T+1, set p_i^{T+1} to a member within the $M \times M$ neighborhood of p_i^T that minimizes $E(p_i)$ for all p_i.
3. Repeat step 2 until the stopping criteria is met.

2.3. Kalman Snake

A common problem with the standard snake finding algorithm is its reliance on image forces during the process of capturing the true contour. The result is that the contour tracking is often ineffective if the snake ever finds itself in a homogeneous region. An obvious solution is to estimate the location of the boundary using a Kalman filter [17] and then position the snake in the proximity of the estimate. The Kalman filter assumes that the dynamic system can be modeled using a linear set of equations represented by the following customary notation:

$$\begin{aligned} x_t &= Ax_{t-1} + w \\ z_t &= Hx_t + v \end{aligned} \tag{2}$$

where x_t and z_t are, respectively, the estimated state of the system and the measurement generated at time t. The state transition matrix A describes the relationship between the current state and the previous state and the measurement matrix H relates the current measurement to the current state. The process noise w and measurement noise v are modeled as zero-mean Gaussian random variables with standard deviation q and r, respectively. The entities A, H, w, and v are chosen to be time-invariant in order to facilitate the implementation of the model.

The Kalman filter assumes that the object boundary can be approximated as an ellipse. This restriction simplifies the state representation since all that is required are the parameters (a, b, c, d, f, g) of the general quadratic equation (Equation (3)) for an ellipse.

$$ax^2 + 2bxy + cy^2 + 2dx + 2fy + g = 0 \tag{3}$$

In addition to the ellipse parameters, the changes in the ellipse parameters are also included in the state equation in order to model the movement of the contour. Hence, the state variable x_t can be represented as a 12-dimensional vector. The state transition matrix A is easily derived from the set of equations relating each state variable in one frame with the corresponding state variable in the subsequent frame (i.e. $a_t = a_{t-1} + \delta a_{t-1}$ and $\delta a_t = \delta a_{t-1}$).

The ellipse parameters are the measured variables and thus, a 6-dimensional vector is used to represent the measurement variable z_t.

The Kalman snake, developed by [16], uses a Kalman filter to estimate the movement, and consequently the location, of the contour. The Kalman snake requires an initial state x_0 and state covariance matrix P_0 to commence the recursive snake finding algorithm. The Contour Tracker treats the user-generated initial snake as the starting state x_0. The choice of x_0 is reasonable since the user will presumably initialize the snake finding algorithm with a high-quality preliminary snake. The state covariance matrix P_0 is set with values determined from experimental data generated using a standard snake.

The Kalman snake begins with the a priori prediction of the current state x_t^- based on the previous state x_{t-1}. A measurement z_t is generated by running the snake finding algorithm, on frame f_t, starting with the ellipse described by the parameters in x_{t-1}. The next step is to combine x_t^- and z_t to update the Kalman filter's a posteriori estimate x_t. After the Kalman filter has generated the current state x_t, the snake algorithm is performed on frame f_t using x_t as the initial snake. The steps are repeated iteratively until all frames have been processed.

2.4. Gradient Vector Flow

Although the Kalman snake resolves the initialization problem; its main drawback is that it is designed to model linear systems. A contour whose movement is not representative of a linear model will not benefit from using the Kalman snake algorithm described above. Xu and Prince [18] propose the gradient vector flow (GVF) field as an alternative solution to the initialization problem. The GVF targets the external energy term of the snake equation. In traditional snakes, computation of the external energy term typically involves standard edge detection algorithms that use the gradient or Laplacian operators. The GVF expands upon these approaches by using the edge maps to detect the changes in the gradient. The GVF field is the vector field $\mathbf{v}[u(x,y), v(x,y)]$ that minimizes the energy functional defined in Equation (4).

$$\begin{aligned} E(\mathbf{v}) &= \int\int \mu(u_x^2 + u_y^2 + v_x^2 + v_y^2) \\ &\quad + |\nabla f|^2 |\mathbf{v} - \nabla f|^2 dxdy \end{aligned} \tag{4}$$

where f is an edge map (or gradient magnitude map) of the original gray-scale image $I(x,y)$ (i.e. $f(x,y) =$

$|\nabla I(x,y)|^2$). In Equation (4), one can notice that the second term dominates in areas of high discontinuities (associated with large values of $|\nabla f|$), whereas the first term dominates in homogeneous regions. The result is a gradual dispersion of the gradient vectors away from object boundaries. This property of the GVF assists the snake algorithm in capturing the contour because it extends beyond the distance afforded by standard gradient-based vector fields.

2.5. Droplet Parameter Extraction

Given the ellipse parameters of the droplet boundary from each frame, certain features of the droplet contour can be computed such as the center point (x_0, y_0), the major and minor axis radii (a' and b'), and the angle of rotation of the major axis (θ).

3. Description of Experimental Setup

The nanostructured surface used for the current study is comprised of Silicon nanorods and was prepared by a process of *glancing angle deposition* (GLAD). A detailed description of the GLAD process is beyond the scope of this paper, but is discussed in [5, 12, 13, 19]. Briefly, in the GLAD process, an RCA-1 cleaned *p*-type Silicon (100) substrate is installed in an electron beam evaporation system (Torr International, Inc.), in such a way that the normal to the substrate surface makes an angle $\theta = 86°$ with the incoming vapor. The evaporation system is then pumped down to a base pressure of around 10^{-6}–10^{-7} Torr. During the vapor deposition, a stepper motor rotates the substrate azimuthally about its surface normal at an angular speed of $0.05rev/sec$. The film thickness and deposition rate are monitored using a quartz crystal microbalance (QCM).

The Silicon nanorods prepared through the GLAD process were vertically aligned on the substrate. The spatial distribution of the nanorods was observed to be statistically uniform. Figure 2 shows images, of the top-view and cross-sectional view of the nanosurface, obtained from a scanning electron microscope (SEM). The inter-nanorod separation distances and the heights of the nanorods are easily controllable. The morphological parameters obtained from the SEM images are as follows: the average diameter of the nanorods at the top of the nanostructured surface $d_t = 133 \pm 34nm$, the average inter-nanorod separation distance $L = 280 \pm 106nm$, and the average nanorod height $h = 1106 \pm 104nm$. For the purpose of measurement and analysis of the dynamics of wettability, a $3\mu L$ water droplet was dispensed through a $250\mu L$ Hamilton syringe onto a sample of the freshly prepared nanostructured surface. A very slow approach speed was utilized in order to minimize the effect of the impact of the water droplet on the surface. The video of the dynamics of the spreading droplet was taken with a fast CCD camera (Pyramid Imaging Inc.) and recorded using the XCAP software (EPIX, Inc.). During the entire experiment, the temperature was maintained at $\sim 25°C$ and the humidity was maintained at $\sim 23\%$.

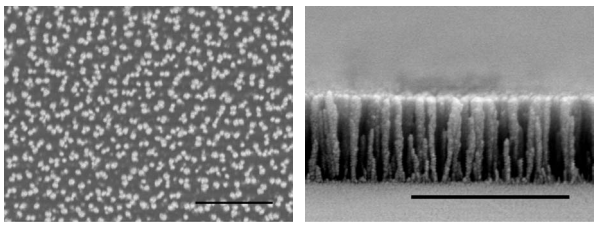

(a) (b)

Figure 2. (a) Top-view and (b) cross-sectional view of Silicon nanorods grown by glancing angle deposition (GLAD). The deposition rate was $0.2nm/sec$. The scale bar is $2\mu m$.

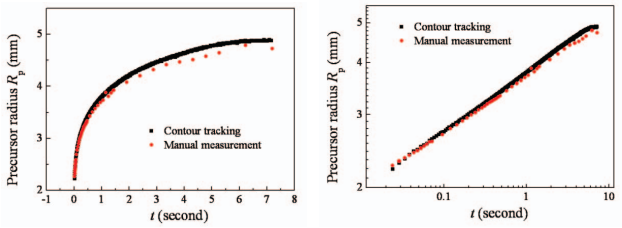

(a) (b)

Figure 3. Comparison of the evolution of the precursor radius R_p over time t calculated from manual measurement and using the *Contour Tracker* on a (a) linear scale and (b) log-log scale.

The Contour Tracker application was developed using the Open Source Computer Vision (OpenCV) Library (introduced by Intel Corporation), in conjunction with Microsoft's Visual C++ .Net architecture. The application employs the snake algorithm to track a single contour within a video or sequence of frames. The current version features the two aforementioned common variations of snake tracking algorithms: the standard snake developed by [8] and the Kalman snake developed by [16]. Four additional external energy operators are included for added functionality. They are the Sobel operator, the Canny operator, edge detection with embedded confidence [11], and the gradient vector flow field [18].

The outputs of the program are a tab-delimited text file specifying the ellipse parameters (a through g) and droplet features (center point, major and minor axes, and rotation

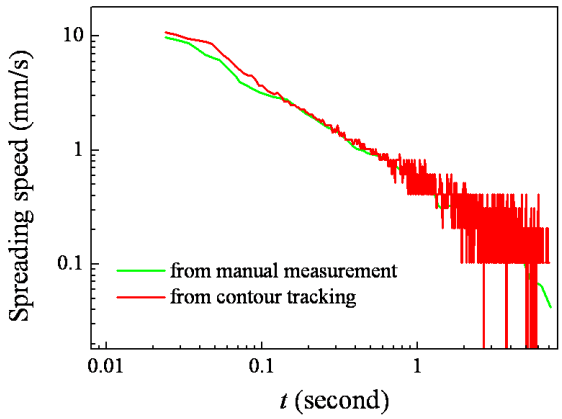

Figure 4. The instantaneous spreading speed of the precursor radius obtained from the temporal differentiation of the curves in Figure 3 followed by a 5-adjacent point smoothing procedure.

angle of the major axis) for each frame, as well as a video displaying the estimated location of the contour.

4. Results and Analysis

Figure 3 shows a comparison of the precursor radius R_p obtained through manual measurement and determined by the *Contour Tracker*. We can observe that manual measurement provides a limited number of data points, some of which are unacceptable, whereas the contour tracking program provides a smooth plot. Linearization of the two curves using a log-log scale (Figure 3(b)) for values of $t < 3.5$ seconds yields two different values for the scaling exponent α: 0.136 resulting from manual measurement and 0.146 resulting from the contour tracking program. Table 1 compares the precursor radius at three different time instances as obtained from manual measurements and the *Contour Tracker*. Figure 4 plots the evolution of the instantaneous droplet spreading speed, which is obtained simply via the temporal differentiation of the curves in Figure 3 followed by a 5-adjacent point smoothing procedure. For small values of t, the values of the instantaneous droplet spreading speed resulting from manual measurement and the contour tracking program differ; this can be attributed to measurement accuracy. However, for large values of t, we observe that the speed from the contour tracking is very noisy. The fact is, for large values of t, the change in the precursor radius from one frame to the next is very small (less than one pixel for a single frame interval). However, since the current version of the contour tracking program only outputs integer values for the contour position it is not well-suited from a metrological standpoint for cases where the changes in contour position are very small. Subpixel interpolation techniques are called for under these circumstances.

Time (second)	0.053	1.055	5.273
Manual (mm)	2.491	3.731	4.639
Contour Tracker	2.513	3.829	4.819
Percent difference (%)	0.9	2.6	3.7

Table 1. Comparison of the precursor radius R_p obtained from manual measurements and the *Contour Tracker* at 3 time instances.

The contour tracking program is further tested on an example of water spreading anisotropically on a sample surface comprised of tilted Si nanorods. We placed a $2\mu L$ water drop onto this surface, and recorded the spreading process with the same CCD camera. Figure 5 shows the evolution of the drop where initially the drop spread along the tilting direction of the nanorods. As the spreading progressed, the drop became near circular in shape. The tracking results are plotted in Figure 6, in which the insert shows the orientation change of the major axis of the elliptical contour. This tracking result gives a very clear picture of the water droplet dynamics, and thus will facilitate further theoretical analysis.

5. Conclusions and Future Work

Dynamic wettability measurement and analysis of a solid nanostructured surface is a topic of great importance in a variety of problem areas. The dynamic wettability analysis is performed by measuring the evolution of the precursor (outer rim) contour of the water droplet as it spreads on a solid nanostructured surface. We developed a computer program based on the snake active contour model which is capable of precisely tracking the precursor contour of a

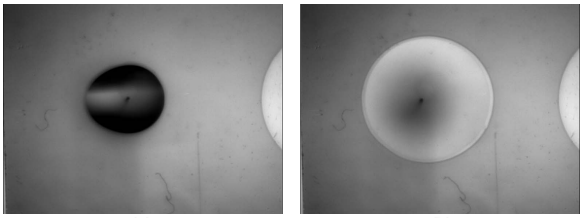

Figure 5. Water drop spreading on the tilted Si nanorod surface. (a) Initial shape (b) Late stage shape

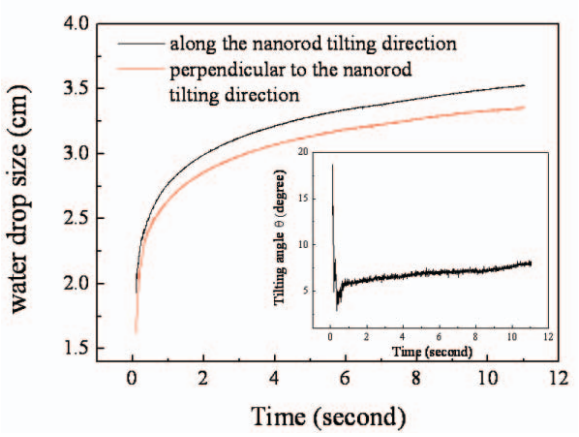

Figure 6. Water drop radius over time. Insert shows the shifting of the major axis of the elliptical shape

spreading water droplet in a high frame-rate video. Experiments show reasonable agreement between the results of the tracking program and those obtained via manual measurement. However, the current version of the contour tracking program is only able to detect the outer rim or precursor contour of the water droplet. This alone is not enough to describe the dynamics of the spreading behavior of the droplet. A fair comparison of the dynamics of water droplet spreading on a nanostructured surface to that on a flat, rough or porous surface requires information about the contact line and hence the length between the contact line and the precursor as a function of time. This calls for being able to track the evolution of the contact line. The contour tracking algorithm also needs to provide sub-pixel accuracy in cases where the differences in contour pixel locations from one frame to the next are very small. These research tasks will be pursued in our future work.

References

[1] M. Apel-Paz and A. Marmur. Spreading of liquids on rough surfaces. *Colloids and Surfaces A: Physiochemical and Engineering Aspects*, 146(1):273–279, 1999.

[2] L. Bacri and F. Brochard-Wyart. Droplet suction on porous media. *European Physical Journal E - Soft Matter*, 3:87–97, 2000.

[3] A. M. Cazabat and M. A. C. Stuart. Dynamics of wetting on smooth and rough surfaces. *Colloid and Polymer Science*, 74(1):69–75, 1987.

[4] A. A. Darhuber, S. M. Troian, and W. W. Reisner. Dynamics of capillary spreading along hydrophilic microstripes. *Physical Review E*, 64(3):031603, 2001.

[5] J. G. Fan, X. J. Tang, and Y. P. Zhao. Water contact angles of vertically aligned si nanorod arrays. *Nanotechnology*, 15:501–504, 2004.

[6] P. G. D. Gennes. Wetting: statics and dynamics. *Reviews of Modern Physics*, 57(3):827–863, 1985.

[7] S. Gerdes, A. M. Cazabat, G. Ström, and F. Tiberg. Effect of surface structure on the spreading of a pdms droplet. *Langmuir*, 14(24):7052–7057, 1998.

[8] M. Kass, A. Witkin, and D. Terzopoulos. Snakes: Active contour models. *International Journal of Computer Vision*, 1(4):321–331, 1988.

[9] K. K. S. Lau, J. Bico, K. B. K. Teo, M. Chhowalla, G. A. J. Amaratunga, W. I. Milne, G. H. McKinley, and K. K. Gleason. Superhydrophobic carbon nanotube forests. *Nanoletters*, 3(12):1701–1705, 2003.

[10] G. McHale, N. J. Shirtcliffe, S. Aqil, C. C. Perry, and M. I. Newton. Topography driven spreading. *Physical Review Letters*, 93(3):036102, 2004.

[11] P. Meer and B. Georgescu. Edge detection with embedded confidence. *IEEE Transactions on Pattern Analysis and Machine Intelligence*, 23(12):1351–1365, 2001.

[12] K. Robbie and M. J. Brett. Sculptured thin films and glancing angle deposition: Growth mechanics and applications. *Journal of Vacuum Science & Technology A: Vacuum, Surfaces, and Films*, 15(3):1460–1465, 1997.

[13] J. C. Sit, D. Vick, K. Robbie, and M. J. Brett. Thin film microstructural control using glancing angle deposition by sputtering. *Journal of Materials Research*, 14:1197–1199, 1999.

[14] V. M. Starov, S. A. Zhdanov, S. R. Kosvintsev, V. D. Sobolev, and M. G. Velarde. Spreading of liquid drops over porous substrates. *Advances in Colloid and Interface Science*, 104:123–158, 2003.

[15] L. H. Tanner. The spreading of silicone oil drops on horizontal surfaces. *Journal of Physics D: Applied Physics*, 12(9):1473–1484, 1979.

[16] D. Terzopoulos and R. Szeliski. Tracking with kalman snakes. In *Active Vision*, pages 3–20. MIT Press, 1993.

[17] G. Welch and G. Bishop. An introduction to the kalman filter. Technical report, University of North Carolina at Chapel Hill, 1995.

[18] C. Xu and J. L. Prince. Snakes, shapes, and gradient vector flow. *IEEE Transactions on Image Processing*, 7(3):359–369, 1998.

[19] Y. P. Zhao, D. X. Ye, G. C. Wang, and T. M. Lu. Designing nanostructures by glancing angle deposition. *Proceedings of the 48th SPIE Conference*, 5219:59–73, 2003.